Lamb Wave Propagation in Monocrystalline Silicon Wafers

Running title: Lamb Wave Propagation in Silicon Wafers

P. Fromme [1], M. Pizzolato [2], Jean-Luc Robyr [2], and B. Masserey [2]

[1] Department of Mechanical Engineering, University College London, WC1E 7JE, UK

[2] Department of Mechanical Engineering, University of Applied Sciences, Fribourg, Switzerland

Correspondence: ++44 207 679 3944 (Phone); p.fromme@ucl.ac.uk

Abstract:

Monocrystalline silicon wafers are widely used in the photovoltaic industry for solar panels with high conversion efficiency. Guided ultrasonic waves offer the potential to efficiently detect micro-cracks in the thin wafers. Previous studies of ultrasonic wave propagation in silicon focused on effects of material anisotropy on bulk ultrasonic waves, but the dependence of the wave propagation characteristics on the material anisotropy is not well understood for Lamb waves. The phase slowness and beam skewing of the two fundamental Lamb wave modes A_0 and S_0 were investigated. Experimental measurements using contact wedge transducer excitation and laser measurement were conducted. Good agreement was found between the theoretically calculated angular dependency of the phase slowness and measurements for different propagation directions relative to the crystal orientation. Significant wave skew and beam widening was observed experimentally due to the anisotropy, especially for the S_0 mode. Explicit Finite Element (FE) simulations were conducted to visualize and quantify the guided wave beam skew. Good agreement was found for the A_0 mode, but a systematic discrepancy was observed for the S_0 mode. These effects need to be considered for the non-destructive testing of wafers using guided waves.

Keywords:

Non-contact Laser Measurement, Guided Ultrasonic Waves, Anisotropy, Wave Beam Skew

PACS:

43.35.Zc, 43.20.Mv, 43.35.Cg

I. Introduction

Solar photovoltaics has become an important source for renewable electricity production. The development of silicon solar cell modules relies on the production of thin wafers with high conversion efficiency. In practice, the minimum thickness during production is limited by the wafer breakage rates[1]. The cutting process induces micro-cracks on the wafer surface. Based on their sensitivity for micro-crack detection, acoustic and ultrasonic methods have been considered for in-line monitoring of the wafers during the manufacturing processes. Scanning acoustic microscopy at frequencies up to 250 MHz was used for the detection of surface cracks as small as 10 μm [2]. Belyaev et al.[3] proposed a resonance ultrasonic vibration technique for fast crack detection in silicon wafers. Frequency shift and bandwidth changes of longitudinal vibration modes were used as indicators of millimeter size cracks. Guided wave approaches were proposed for rapid inspection of silicon wafers[4]. Chakrapani et al.[5] used air-coupled transducers in pitch-catch configuration to generate the fundamental antisymmetric Lamb wave mode A_0 at 200 kHz in 200 μm thick mono- and polycrystalline silicon wafers and detect cracks. Laser generated Lamb waves were propagated in 525 μm thick monocrystalline silicon wafers to detect and estimate the size of 5 mm long artificial cracks[6].

Guided ultrasonic waves can propagate over long distances for the inspection of large structures such as plates or pipes[7-9]. High frequency guided wave methods were employed to detect surface cracks in isotropic metallic plates[10] and perform in-situ monitoring of fatigue crack growth[11]. The propagation of guided ultrasonic waves in anisotropic composite structures has been investigated for aerospace and wind turbine applications. Chapuis et al.[12] investigated the energy radiation of Lamb waves in a thin fiber reinforced composite plate for an axisymmetric source and proposed a far field approximation using Green's function. Numerical and experimental results showed a significant direction-dependent focusing effect of the Lamb modes. Karmazin et al.[13] presented a far-field asymptotic solution for Lamb waves generated in a layered anisotropic plate by a surface-bonded source of finite size. Leleux et al.[14] developed a multi-element matrix ultrasonic probe to inspect large composite plate components in pulse-echo mode from one single position and detect delamination and impact damage. The modal selectivity of the probe and the directivity of the generated ultrasonic field were discussed. For an incident ultrasonic beam on an anisotropic multilayered structure, Potel et al.[15] demonstrated that the Lamb wave beam generated in the plate can deviate with respect to the sagittal plane of excitation towards the stiffer direction of the anisotropic structure.

The propagation of ultrasonic waves in anisotropic materials is characterized by different representative curves (two-dimensional) or surfaces (three-dimensional)[16]. For bulk waves, the phase velocity surface and the slowness surface (inverse of phase velocity) can be calculated by solving the Christoffel equation as a function of the wave normal. The values of these wave parameters give an estimation of the material stiffness directional dependency. The ray or group velocity surface is more difficult to calculate since analytical relations cannot be found in all directions. The direction of the group velocity vector is normal to the slowness surface at that point and the angle between wave vector and the acoustic ray is characterized by the skew angle[17]. The direction dependency of the group velocity for bulk wave propagation in thick silicon discs has been investigated theoretically and experimentally, pointing out the complicated cusps and folding of the ray surface[18]. Audoin et al.[19] presented an approach to recover the stiffness coefficients of anisotropic media from the measured group velocity surface, implementing a signal processing technique to measure the arrival time of each generated wave. Analytical equations relating group velocity to stiffness constants were proposed for arbitrary planes in transversely isotropic materials[20]. Reverdy and Audoin developed a phase velocity based method allowing for the determination of the elastic constants of anisotropic materials by means of laser ultrasonic techniques[21]. Maris investigated the phenomenon of energy focusing due to elastic anisotropy for bulk wave propagation in crystals and proposed an explicit expression to evaluate the enhancement of energy flow in the principal directions[22].

Lamb wave propagation in anisotropic plate structures can be described by the same characteristic parameters. Group velocity curves in thin anisotropic, carbon fiber-reinforced epoxy laminates with thicknesses of approximately 150 μm were measured using a point-source point-receiver configuration and compared to theoretical curves[23]. As the ratio of wavelength to specimen thickness was large, the Lamb wave propagation was described in terms of in-plane longitudinal and shear membrane waves, considering plane wave propagation. The influence of the anisotropy on Zero Group Velocity (ZGV) Lamb modes was investigated in monocrystalline, 525 μm thick silicon wafers using a line laser source with a spectrum limited to 18 MHz [24]. The results demonstrated the amplitude and frequency dependency of the ZGV modes as a function of the excitation orientation and a deviation of the acoustic beam for directions between the principal crystallographic axes. Slowness surface measurements of leaky Lamb waves for silicon wafers immersed in water have been performed[25].

This contribution presents a systematic analysis of the effect of anisotropy on Lamb wave propagation in monocrystalline silicon wafers by means of measurements and Finite Element (FE) simulations. The fundamental antisymmetric and symmetric Lamb modes A_0 and S_0 were generated in monocrystalline silicon wafers using angle beam transducers and the ultrasonic field was measured by means of laser interferometry. The phase slowness curve was measured in the far field of the transducer and compared with theoretical values. The guided wave beam skew was investigated experimentally and compared to FE results and theoretical predictions.

II. Theoretical background

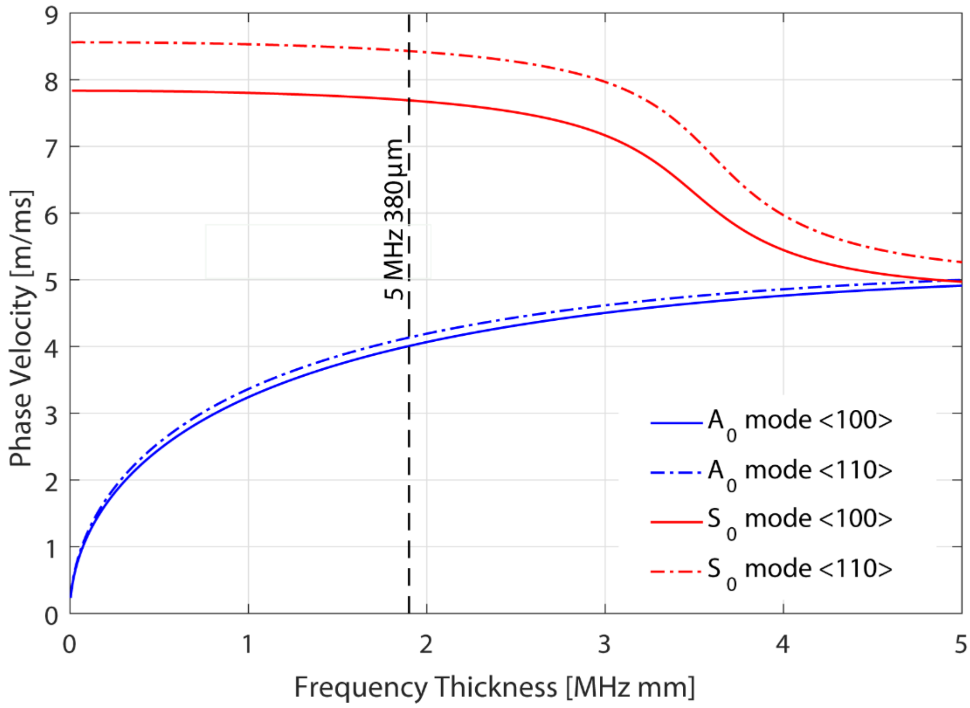

Fig. 1 (color online): Phase velocity dispersion diagram for A_0 and S_0 Lamb wave modes, propagation in silicon wafer in <100> (solid) and <110> (dash-dotted) crystal directions; measurements conducted at 5 MHz center frequency in 380 μm thick wafer (vertical dashed).

Monocrystalline silicon is an orthotropic material characterized by three cubic symmetric stiffness constants. Standard values were taken from literature[26] as C_{11} = 165.7 GPa, C_{12} = 63.9 GPa, and C_{44} = 79.6 GPa. Stiffness constants can decrease from 1% - 3% for higher levels of doping. However, this effect is usually ignored for engineering calculations[26]. The constants were determined for <100> crystal orientation, corresponding to an azimuth angle 0°. In contrast to other anisotropic engineering materials, silicon has a 45° symmetry of the material properties, with a stiffness variation in the order of 15% between the principal <110> direction with the highest stiffness and the principal <100> direction with the lowest stiffness[26]. Theoretical calculation of the phase velocity of the fundamental Lamb modes as a function of the angular orientation of the silicon crystal was performed for a 380 μm thick silicon wafer using Disperse[27] and is shown in Fig. 1. The phase velocity at 5 MHz for the antisymmetric A_0 mode changes by about 3% between crystal directions, and the phase velocity of the symmetric S_0 mode by about 10%. The wavelength λ for the A_0 mode (approximately 0.8 mm) and for the S_0 mode (approximately 1.6 mm) change by the same percentage between propagation directions. Often the phase slowness, the inverse of the phase velocity, is used to display the propagation velocity variation in function of the crystallographic orientation. The wave skew for any phase direction can be visualized as the normal direction to the phase slowness curve[17].

III. Experiments

Polished monocrystalline (001)-cut silicon wafers were used to measure the phase slowness and beam skew of the fundamental Lamb wave modes A_0 and S_0. The P-type silicon specimens were boron doped and had a diameter of 100 mm (4 inch) and nominal thickness of 380 µm. Within the (001) plane of the wafer, the material properties are identical every 90°. The principal direction with the lowest stiffness [100] was labelled as 0°, the principal direction with highest stiffness [110] as 45°, with 90° corresponding to the [010] principal direction with lowest stiffness (identical to [100] direction). The wave modes were excited using a commercial piezoelectric transducer with 5 MHz center frequency (Harisonic ABM0504 5MHz). The transducer was attached to custom-made Nylon wedges (8.5 mm width) with the angle adapted to excite selectively the A_0 mode (41° wedge angle) or the S_0 mode (19° wedge angle) according to Snell's law and nominal phase velocity values for propagation in the <110> direction. Both the silicon wafer and transducer were fixed in custom-made holders to achieve accurate positioning and defined contact pressure between the wedge and the wafer. The angle beam wedge transducer was coupled to the wafer using liquid ultrasonic couplant, with excess couplant on the wafer surface removed. The wedge was pressed down with a defined force of approximately 10N by setting the compression length of a spring, calibrated in advance. The contact force was selected in a force range where limited variation of the guided wave amplitude was observed, but low enough to limit the risk of wafer breakage. For measurements in different directions relative to the crystallographic orientation, the wafer holder allowed angular adjustments with an accuracy of approximately 1°.

The excitation signal was defined as a sinusoidal toneburst with 12 cycles and 5 MHz center frequency using an arbitrary function generator (Agilent 33220A). The signal was amplified to approximately 400 V_{pp} using a power amplifier (RF 1020L) and applied to the piezoelectric transducer. This allows good control over the frequency content of the excited narrowband guided wave pulse to reduce dispersion with limited pulse time length. The out-of-plane displacement was measured using a non-contact laser interferometer (Polytec OFV-5000 and OFV 505). Measured time series were band-pass (2 to 7 MHz) filtered (KH 3945), averaged 50 times, and recorded using a digital storage oscilloscope (LeCroy 9304). The laser interferometer was fixed to a 2 axis scanning rig and moved parallel to the wafer, keeping the laser beam perpendicular to the polished wafer surface.

The phase velocity was measured in the transducer far field on the center line of the wedge, at a distance of 42 mm from the angle beam transducer. The measurements were performed over a straight line of 10 mm with measurement steps every 0.2 mm, in total 51 measurement points (Fig. 2). The silicon wafer was rotated using the holder in 5° angular steps from the [100] (0°) crystal direction via the [110] (45°) direction to the [010] (90°) crystallographic direction and measurements taken. Hilbert transform was applied to the time trace for each measurement point to extract the arrival time of the signal peak and calculate the group velocity c_g. Based on the group velocity, the time trace was windowed for each spatial step to contain only the incident wave mode of interest. Fast Fourier Transform (FFT) was used to extract the phase value of the time trace for every measurement point. After removal of 2π phase jumps, the phase variation as a function of the spatial measurement step was fitted with a linear function to calculate the phase velocity c_p for each propagation direction.

For the beam skew experiments the laser measurement was performed over a two-dimensional area, recording the guided wave signal on 9 parallel lines (5 mm steps) perpendicular to the expected beam propagation direction (excitation center line) over a length of 40 mm in front of the transducer. Each line had 21 steps of 1 mm (Fig. 2). For each measurement point the amplitude of the guided wave pulse was extracted after time windowing using FFT and recorded. Beam skew experiments were conducted for both fundamental Lamb wave modes for 4 orientations of the silicon wafer (0°, 15°, 30°, 45°).

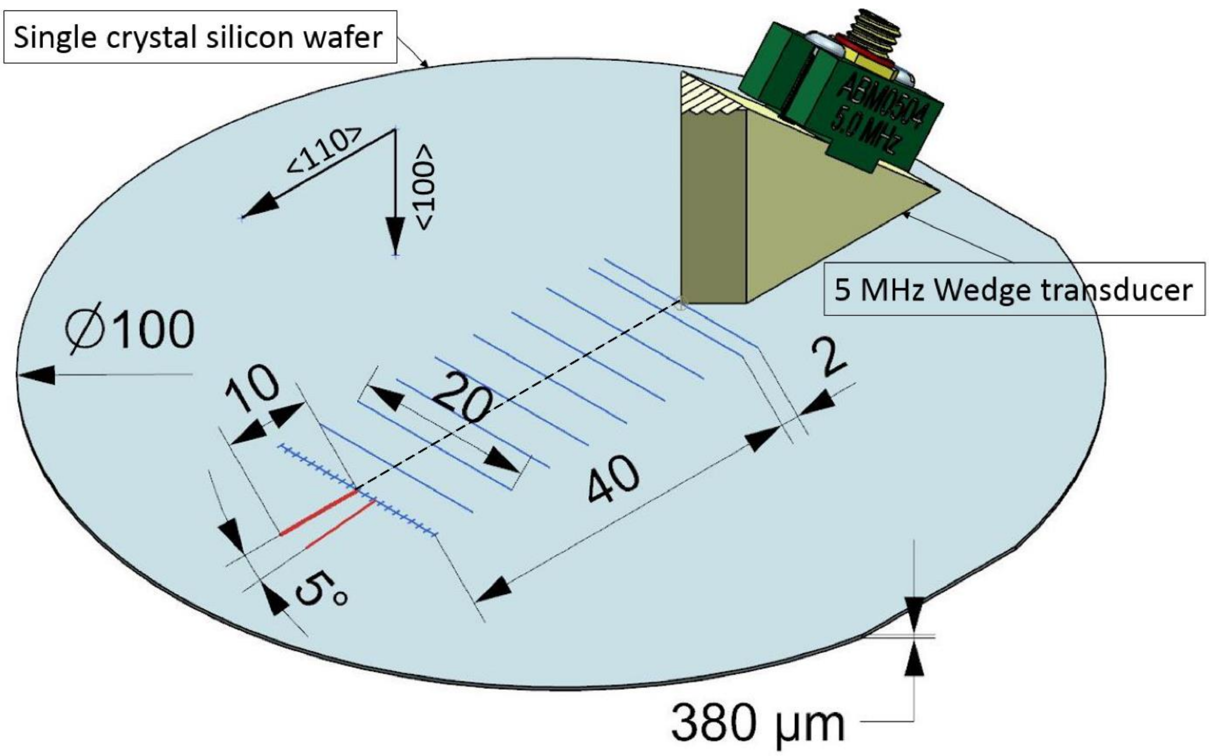

Fig. 2 (color online): Schematic representation of the experimental setup showing (100) silicon wafer (diameter 100 mm, thickness 380 μm), angle beam wedge transducer, laser measurement area for beam skew (40 mm x 20 mm) and line for phase velocity (10 mm).

IV. Phase slowness

The theoretical phase slowness curves were predicted using Disperse[27] for the nominal orthotropic material properties of silicon and compared to the measured values (Fig. 3). For the A_0 mode a 3% variation with propagation angle was predicted. The measured values match the theoretical values well and show the expected symmetry to the 45° orientation. For the S_0 mode the variation of the phase slowness with orientation is predicted theoretically to be about 10% and matched from the measurement results in the 0°, 45° and 90° directions. Therefore, the silicon wafer material properties and the relative change in stiffness with crystallographic orientation lie within the range of 1-3% of the nominal properties stated in literature[26]. However, a small but systematic offset in the non-principal directions was found, with higher experimental slowness (lower phase velocity) values than theoretically predicted. For these directions, a significant wave skew of the S_0 mode was observed, leading to low amplitude in the far field of the transducer along the center line where phase velocity was measured. It should be noted that the experimental setup for the S_0 mode excitation, with the transducer wedge width approximately 3 times the wavelength, does not exactly match the theoretical assumptions for plane wave generation, implications of which will be discussed further.

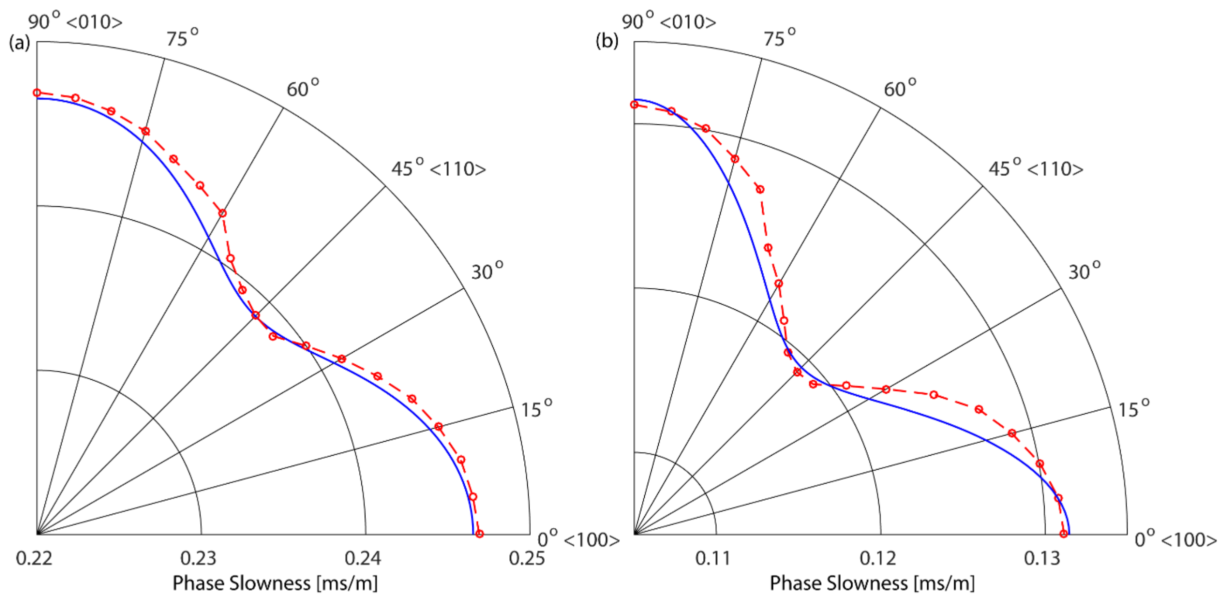

Fig. 3 (color online): Comparison of phase slowness curves at 5 MHz in 380 μm thick monocrystalline silicon wafer; theory (solid) and measurement (dashed, circles): (a) A_0 mode; (b) S_0 mode.

V. Finite Element Simulations

The propagation of the guided wave modes in the silicon wafers was simulated using three-dimensional (3D) Finite Element (FE) models to visualize and better understand the beam skew due to the material anisotropy. The model of a 380 μm thick silicon plate (size: 60 mm x 60 mm) was implemented with approximately 11.5 million linear brick elements ($\Delta x = \Delta y = 50$ μm, $\Delta z = 47.5$ μm) in ABAQUS Explicit, similar to the model described in [28]. Explicit time integration was used, and the element size and time step were chosen to adhere to the usual stability criteria[29]. The element size was chosen small enough compared to the wavelength, using at least 16 elements per wavelength. The orthotropic material properties were specified using the nominal material properties from literature stated above[26]. For simulations of different excitation orientations relative to the principal axis, the material properties were specified with a rotated axis system, keeping the geometry the same. Line excitation of respectively the A_0 and S_0 Lamb wave modes was introduced at one edge of the plate. Approximating the effective transducer width used for the experiments, all nodes over a width of 5 mm at the center of the plate thickness were excited either using in-plane (S_0 mode) or out-of-plane (A_0 mode) force. The amplitude over the 5 mm excitation width was set to vary from 0.5 at the sides to 1 at the center using a Hanning distribution. The excitation pulse was set as a 12 cycle toneburst with a center frequency f of 5 MHz to match the experiments. The amplitude for both modes was monitored as the out-of-plane displacement at the top surface nodes on points in a rectangular area of 40 mm (width step: 1 mm) by 50 mm (length step: 2.5 mm) in front of the excitation to capture the propagation and skew of the guided wave mode pulses. The time trace at each monitoring node was time gated to remove reflections from the plate edges and other modes. Fast Fourier Transform (FFT) was used to extract the amplitude at the center frequency of 5 MHz for each monitoring node.

VI. Wave beam skew visualization

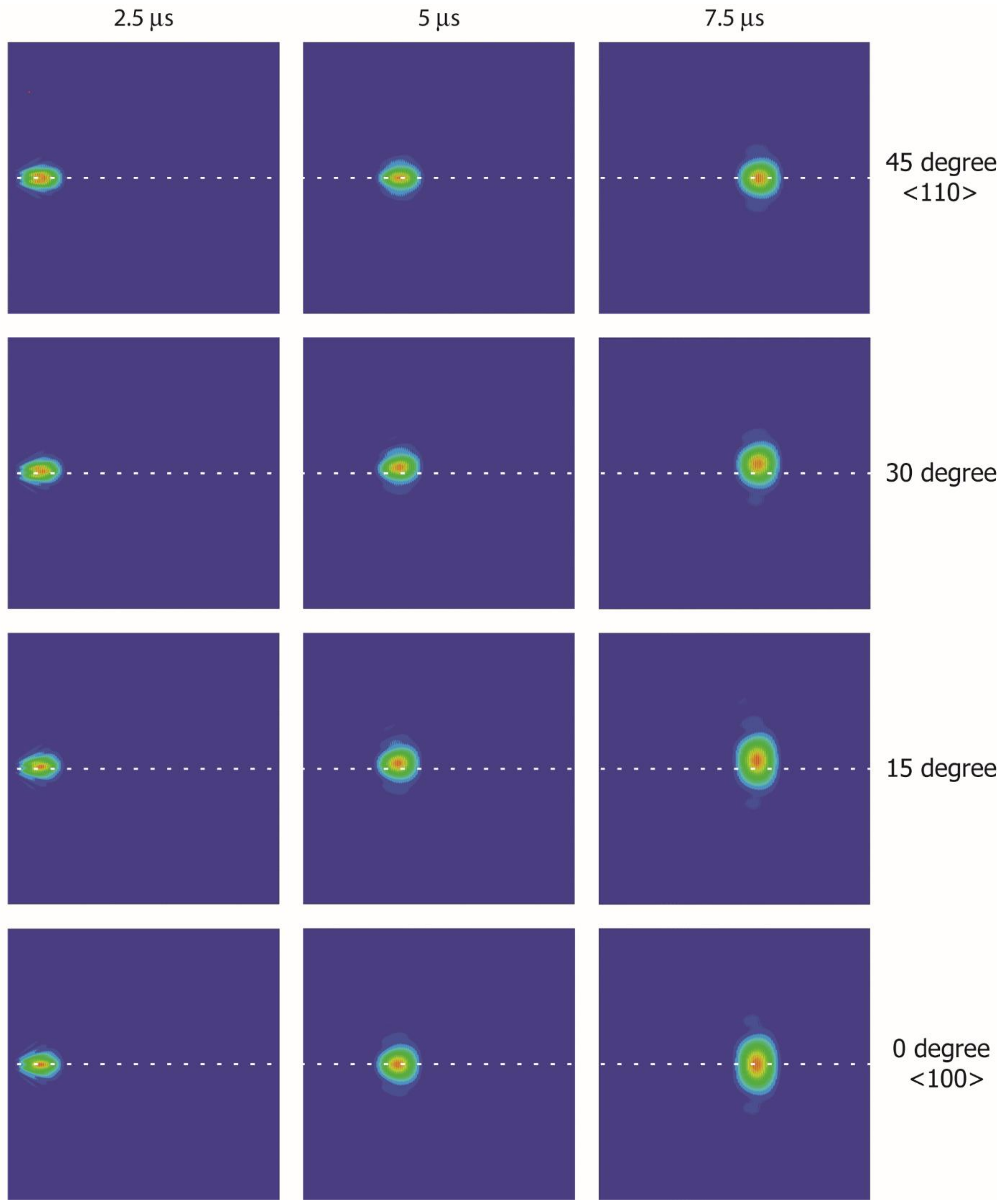

Fig. 4 (color online): Time snapshots of A_0 mode wave propagation, FE simulation at 3 times (2.5, 5.0, 7.5 μs) for different crystallographic orientations relative to line excitation at edge of plate; 60 mm by 60 mm area shown; dashed line: excitation center line.

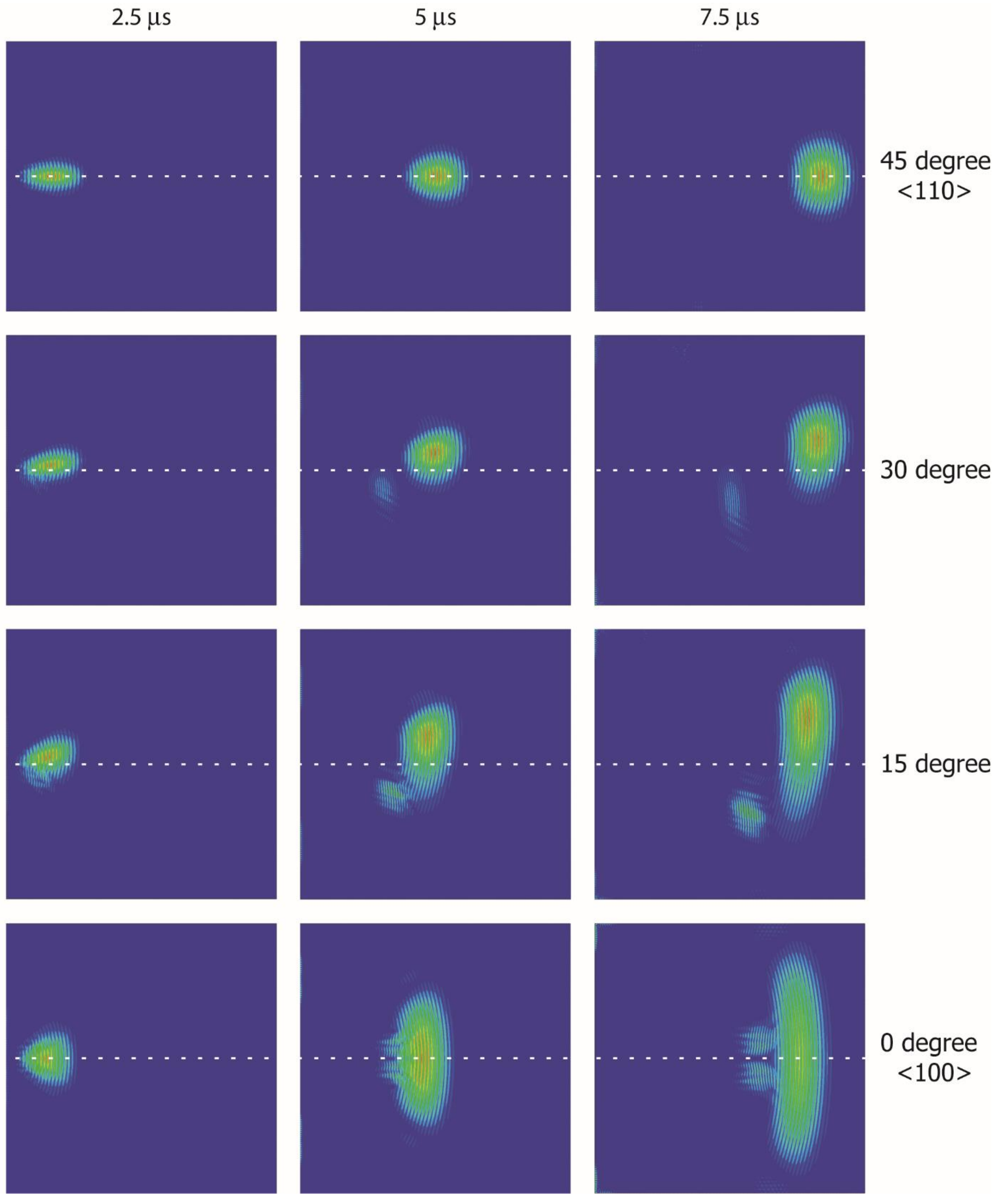

Fig. 5 (color online): Time snapshots of S_0 mode wave propagation, FE simulation at 3 times (2.5, 5.0, 7.5 μs) for different crystallographic orientations relative to line excitation at edge of plate; 60 mm by 60 mm area shown; dashed line: excitation center line.

Figure 4 shows time snapshots of the simulated A_0 mode propagation for different crystallographic orientations relative to the line excitation at the left edge of the plate. As the 5 mm line excitation is relatively long compared to the wavelength of the A_0 mode (approximately 0.8 mm), a rather narrow wave pulse is excited. For the two principal crystallographic directions in the <110> (45°) and <100> (0°) crystal orientations, the wave front remains perpendicular to the excitation line (wave propagation along dashed excitation center line). For the 30° and 15° directions, the excitation center line is not aligned with the material symmetry axes and a slight wave skew can be observed relative to the dashed line. The effect is small for the A_0 mode, as the variation in the theoretical phase slowness is only about 3%, giving a maximum theoretically predicted wave skew angle of 3.6°. Comparing the time snapshots at 7.5 μs, it can be observed that the pulse spreads more in the width direction as the crystallographic orientation moves away from the <110> direction with the highest stiffness.

Figure 5 shows the time snapshots of the simulations for the S_0 mode at the same times as for the A_0 mode in Fig. 3. As the group velocity of the S_0 mode is higher than for the A_0 mode, the pulses have propagated farther. A slight excitation of the SH mode and an edge guided wave were observed for the non-principal orientations due to the mode coupling, and can be seen as the secondary, slower wave pulse for the 30° and 15° direction cases. For the <110> crystal direction, the wave pulse propagates along the excitation center line with only limited pulse spreading. For the S_0 mode, the excitation line length is about 3 times the wavelength (compared to 6 times λ for the A_0 mode), so increased pulse spreading is to be expected. When the excitation direction is not aligned with one of the principal axes of the crystal (30° and 15° orientations), a significant wave skew can be observed, as the phase slowness varies by about 10% for the S_0 mode. Moving away from the <110> direction with the highest stiffness, it can be observed that the pulse spreads perpendicular to the wave propagation direction. This effect can be seen to be the strongest in the <100> orientation, which is a principal axis of the anisotropy, but has the lowest stiffness and thus phase velocity. For this direction, no wave skew, but a slower group velocity and significantly wider pulse spreading than for the <110> orientation are observed. The significant widening of the wave pulse has not been previously reported in literature. The changes of up to 10% in the phase slowness and thus wavelength relative to the excitation aperture cannot explain this significant change in the beam spread angle, which can thus be attributed to anisotropic wave propagation effects further described below, with the largest effect occurring along a principal axis with a minimum of the guided wave velocity (<100>).

As described above, the displacement on a rectangular grid was recorded and the amplitude at each point of the grid evaluated to quantify the excited wave beam. These are shown in Fig. 6 for the FE simulations of the A_0 and S_0 modes. For the A_0 mode a strong beam can be observed for all crystallographic orientations, with a small wave skew for the 15° and 30° directions and a slightly larger beam widening for the 0° direction. The wave skew for the S_0 mode for the 15° and 30° crystallographic orientations is significantly higher. The resulting amplitude field is characterized by an asymmetry of the wave beam with different amplitude drop gradients in the positive and negative perpendicular direction, as can be seen for example in Fig. 6g. The beam widening for the S_0 mode can be clearly seen, with a significantly larger amplitude decrease for the <100> orientation than for the <110> direction (compare Fig. 6h and Fig. 6e). The observed wave skew and beam widening effects can be related to the energy focusing effect discussed in [12] and [14] for composite plates. Based on the shape of the slowness curve for the S_0 mode, the energy is expected to be essentially focused in the <110> direction. The FE results can be compared to the experimental results shown in Fig. 7. Overall a good match can be seen with the same overall effects. For the measurement results, the wave fields for the <110> and <100> directions are not perfectly symmetric, due to uncertainties for the angle of the experimental setup.

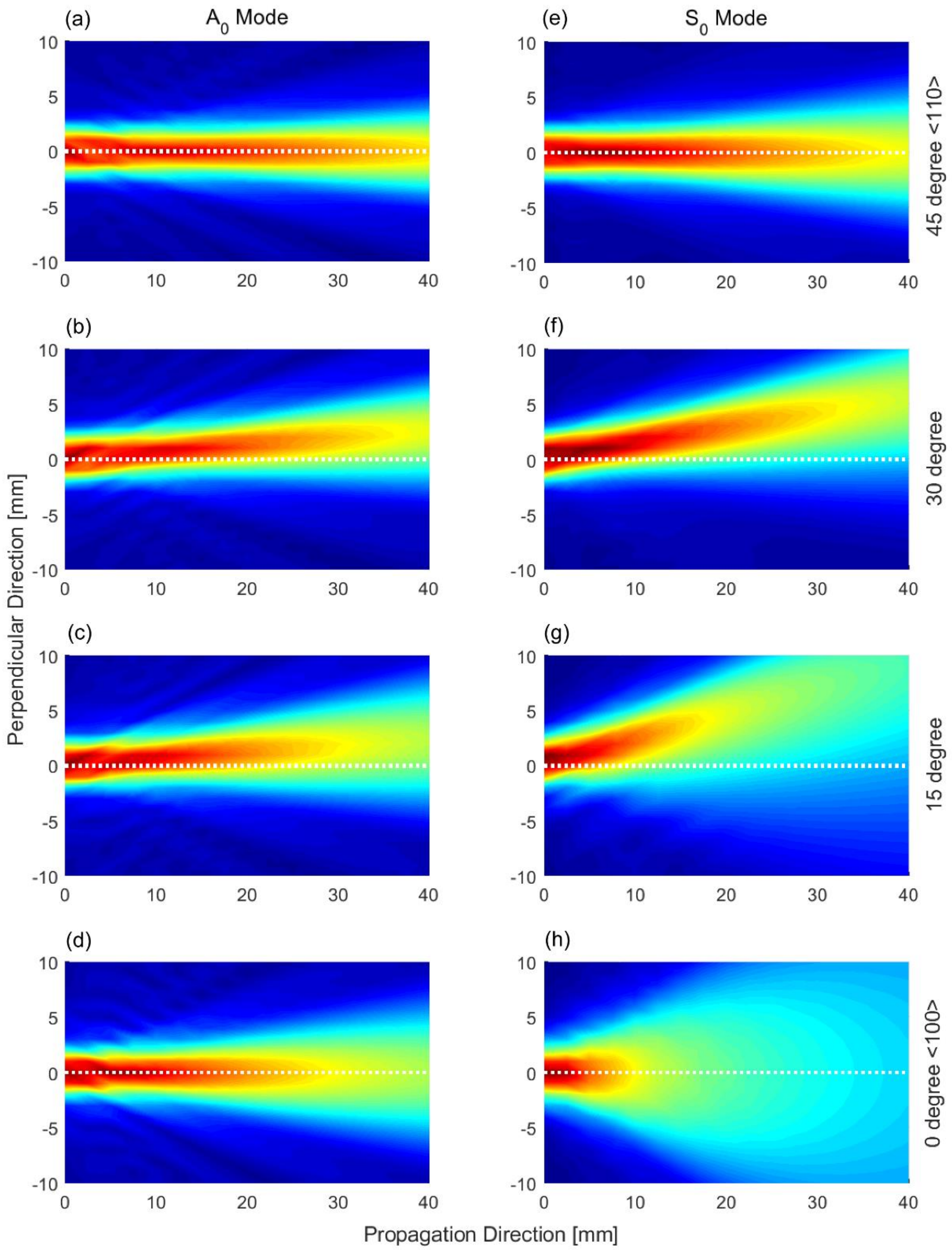

Fig. 6 (color online): FE simulation of beam skewing; evaluation of amplitude (FFT) at each monitoring location for A_0 and S_0 mode, different crystallographic orientations relative to line excitation.

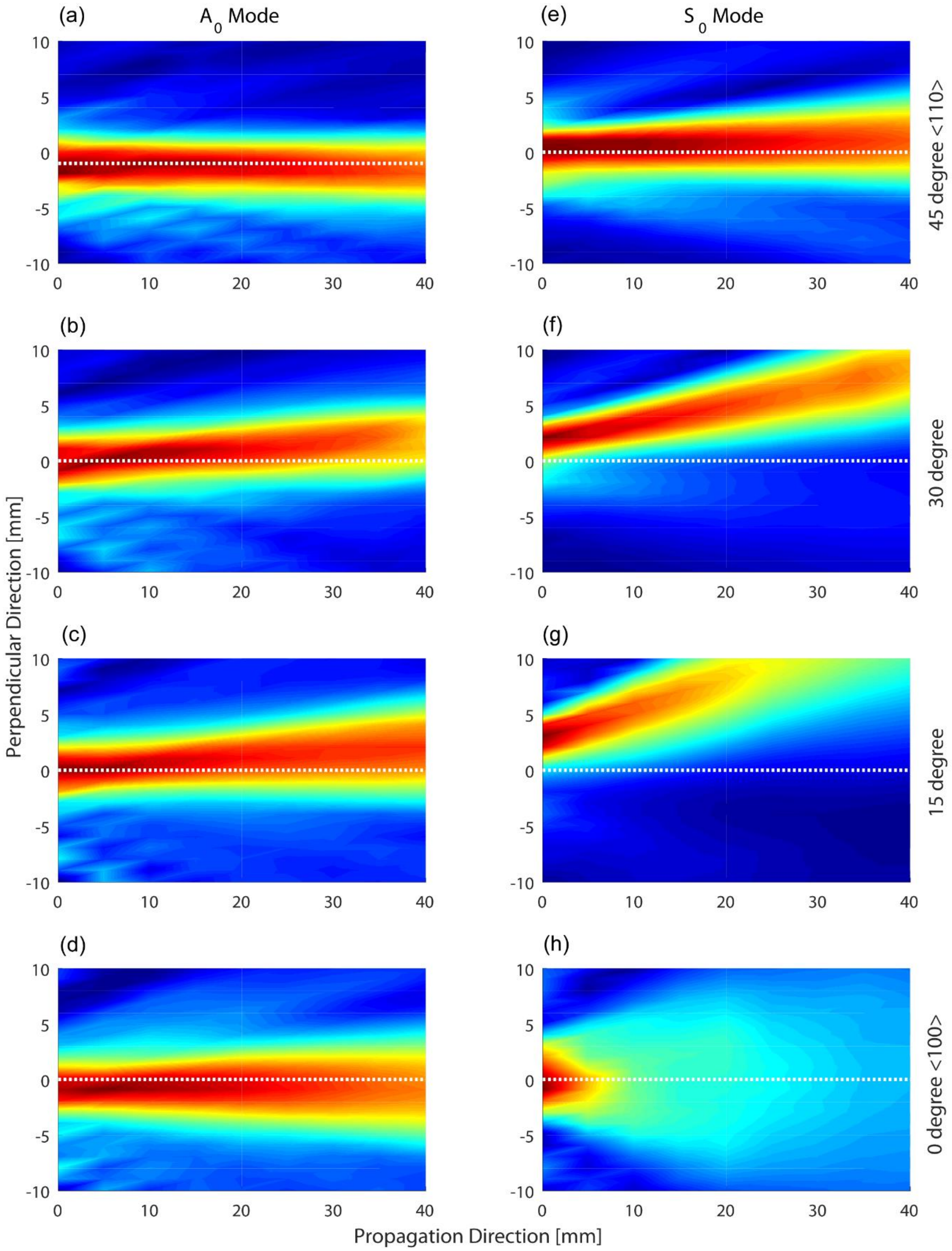

294

295 Fig. 7 (color online): Experimental measurement of beam skewing; evaluation of amplitude
296 (FFT) at each monitoring location for A_0 and S_0 mode, different crystallographic orientations
297 relative to line excitation.

VII. Wave beam skew evaluation

The magnitude and angular dependency of the wave beam skew for the two fundamental Lamb modes, predicted from theoretical calculations, are shown in Fig. 8 (solid line) and Table 1. The maximum skew angle is calculated as 10.6° for the S_0 mode at an orientation angle of 17°, while for the A_0 mode the maximum theoretical skew angle of 3.6° occurs at 24° orientation. The significantly larger wave skew for the S_0 mode is in line with the larger variations of the phase slowness curves (Fig. 3). For the FE simulations and the experiments, the wave skew was evaluated for both Lamb wave modes and all relative crystal orientations (every 5° for FE simulations, every 15° for experiments). The wave skew angle was evaluated by computing the angle between the excitation center line and the trajectory of the acoustic ray with maximum field amplitude[15]. This approach assumes that the wave vector direction in the main acoustic beam is defined by the wedge orientation and is therefore parallel to the excitation center line. Depending on the excitation width, the acoustic ray with maximum amplitude can have a small offset from the acoustic ray with zero phase gradient (relative to the excitation center line), leading to an overestimation of the wave skew angle. For each measurement line perpendicular to the center line, the amplitude was interpolated to a step size of 0.1 mm using a low pass filter in Matlab to accurately evaluate small angles, especially for the A_0 wave mode skew. The location of the amplitude maxima was extracted and a straight line fitted to obtain an approximation of the wave skew angle, discarding the first 5 mm in front of the excitation due to near field effects. Figure 8 shows the obtained wave skew angles for different crystallographic directions.

The experimental and FE simulation results for the A_0 mode match very well with the theoretical predictions (Fig. 8, Table 1). For the A_0 mode results, the skew angle is rather small and a strong beam was observed for all directions in Figs. 6 and 7. No wave skew was observed in the FE simulations for the principal 0° and 45° directions as the wave propagation is perfectly symmetric. For the experimental results, slight asymmetries and beam skew were seen in the principal directions (Fig. 7a/d), and this was found to be up to 0.4° for the A_0 mode (below experimental uncertainty of 1°). For the S_0 mode, both the experimental and FE simulation evaluation show a similar dependency of the skew angle as predicted theoretically, but with a consistent overestimation (Fig. 8, Table 1). No wave skew was observed in the FE simulations for the principal 0° and 45° directions, with experimental results showing a maximum wave skew angle of 1.8°. The evaluation of both experiments and FE simulations gave higher values than predicted for the non-principal directions, but the angular dependency matches well. A preliminary evaluation of the phase gradients obtained from additional FE simulations with a finer grid (not shown) showed small angular offsets in the main acoustic beam between the excitation center line and the wave vector (assumed to be parallel to the center line), leading to an overestimation of the skew angle. The phase gradient analysis also showed that, in the far-field, the wave propagation characteristics of the acoustic beam are closer to a point-like source than to plane wave propagation with parallel rays, which is in line with the short line source employed here. These elements would help to explain the observed systematic offset compared to theory. For the experiments, the spacing of the measurement grid and noise precluded such an evaluation, as the correction for 2π jumps in the wave phase field was problematic. Therefore, a decision was taken to use the same evaluation criterion for both the experiments and FE simulations to allow comparison.

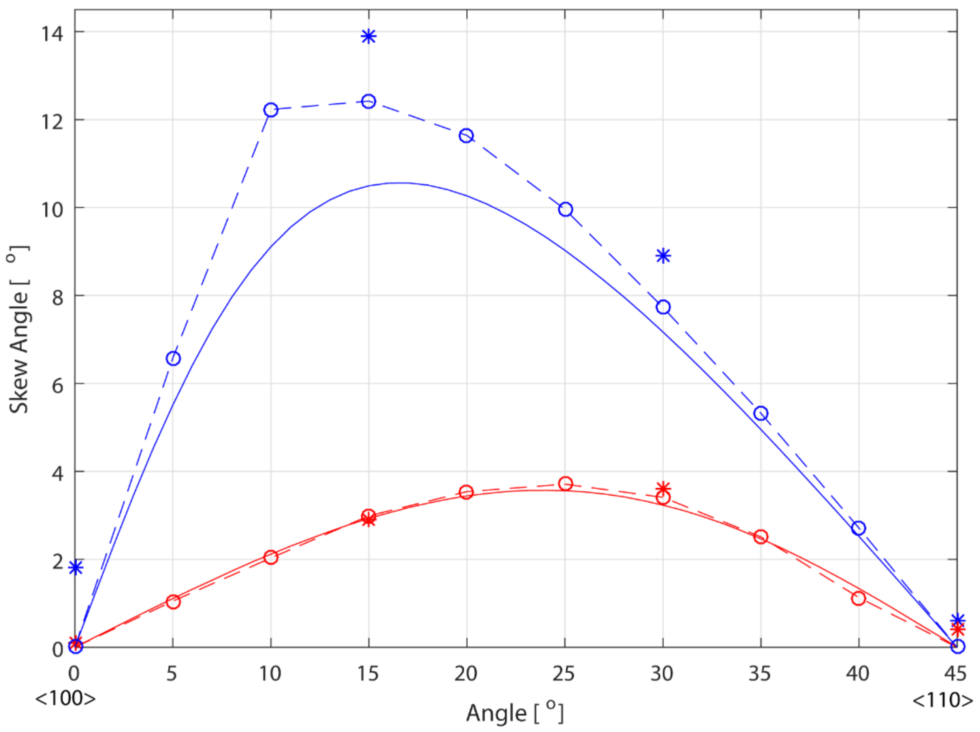

Figure 8 (color online): Comparison of wave skew angle A_0 (red) and S_0 (blue) modes: theory (solid, every 1°), FEA (circles, dashed, every 5°), experiment (stars, every 15°).

Table 1: Comparison wave skew angle A_0 and S_0 modes theory, FE, experiment (experimental uncertainty order of 1°).

Mode	Angle	Theory	FE	Experiment
S_0	0°	0°	0°	1.8°
	15°	10.5°	12.4°	13.9°
	30°	7.2°	7.7°	8.9°
	45°	0°	0°	0.6°
A_0	0°	0°	0°	0.1°
	15°	2.9°	3.0°	2.9°
	30°	3.2°	3.4°	3.6°
	45°	0°	0°	0.4°

VIII. Conclusions

The propagation of the fundamental Lamb wave modes in monocrystalline silicon wafers (380 μm thickness) was investigated. The anisotropic material properties lead to a variation of the phase velocity depending on the propagation direction relative to the crystallographic orientation. The phase velocity was measured experimentally using a customized angle beam transducer for the selective excitation of the guided wave modes, measuring the out-of-plane displacement with a non-contact laser vibrometer. Good agreement of the measured phase slowness curves with theoretical predictions was found. The larger variation of the phase slowness for the fundamental symmetric S_0 mode leads to a significant wave skew angle for propagation in non-principal directions of the silicon crystal. The effect was observed experimentally and verified from FE simulations. Both the experimental and FE simulation evaluation show a similar angular dependency of the skew angle as predicted theoretically, but with a consistent overestimation. This discrepancy may result from the evaluation procedure of the skew angle, based on the acoustic ray with maximum amplitude, and from the short line sources used for the S_0 mode excitation in the simulations and the measurements. In directions with lower stiffness, a significant beam widening was observed, that has not been reported previously in literature. For the A_0 mode the wave skew effect was confirmed and good agreement between experimental measurements, FE simulations, and theoretical predictions was obtained. The wave skew and beam widening can lead to significant amplitude drop in the normal excitation direction and need to be considered for potential non-destructive testing applications for silicon wafers.

Acknowledgements

The authors would like to thank Prof. N. Saffari for the generous provision of experimental equipment.

References

[1] A. Luque and S. Hegedus, *Handbook of Photovoltaic Science and Engineering*, (Wiley, West Sussex, 2011), pp. 239-240.

[2] A. Belyaev, O. Polupan, S. Ostapenko, D.P. Hess, and J. P. Kalejs, “Resonance ultrasonic vibration diagnostics of elastic stress in full-size silicon wafers,” Semicond. Sci. Technol. **21**, 254–260 (2006).

[3] A. Belyaev, O. Polupan, W. Dallas, S. Ostapenko, D. Hess, and J. Wohlgemuth, “Crack detection and analyses using resonance ultrasonic vibrations in full-size crystalline silicon wafers,” Appl. Phys. Lett. **88**, 111907–111909 (2006).

[4] M.J. Padiyar, S.K. Chakrapani, C. V. Krishnamurthy, and K. Balasubramaniam, “Crack detection in polycrystalline silicon wafers using air-coupled ultrasonic guided waves,” in *Proceedings of the National Seminar & Exhibition on Non-Destructive Evaluation* (NDE 2009, Dec. 10–12, 2009), pp. 341–345.

[5] S.K. Chakrapani, M.J. Padiyar, and K. Balasubramaniam, “Crack detection in full size Cz-silicon wafers using Lamb wave air coupled ultrasonic testing (LAC-UT),” J. Nondestr. Eval. **31**, 46–55 (2012).

[6] M.-K. Song, K.-Y. Jhang, “Crack Detection in Single-Crystalline Silicon Wafer Using Laser Generated Lamb Wave,” Adv. Mater. Sci. Eng. **2013**, 950791 (2013).

[7] D. E. Chimenti, “Guided waves in plates and their use in materials characterization,” Appl. Mech. Rev. **50**, 247-284 (1997).

[8] P. Cawley, M.J.S. Lowe, D.N. Alleyne, B. Pavlakovic, and P.D. Wilcox, “Practical long range guided wave testing: applications to pipes and rail,” Mater. Eval. **61**, 66-74 (2003).

[9] J.L. Rose, “Standing on the shoulders of giants: An example of guided wave inspection,” Mater. Eval. **60**, 53-59 (2002).

[10] B. Masserey and P. Fromme, "On the reflection of coupled Rayleigh-like waves at surface defects in plates," J. Acoust. Soc. Am. **123**, 88-98 (2008).

[11] B. Masserey and P. Fromme, "In-situ monitoring of fatigue crack growth using high frequency guided waves," NDT&E Int. **71**, 1-7 (2015).

[12] B. Chapuis, N. Terrien, D. Royer, "Excitation and focusing of Lamb waves in a multilayered anisotropic plate," J. Acoust. Soc. Am. **127**, 198-203 (2010).

[13] A. Karmazin, E. Kirillova, W. Seemann and P.Syromyatnikov, "A study of time harmonic guided Lamb waves and their caustics in composite plates," Ultrasonics **53**, 283-293 (2013).

[14] A. Leleux, P. Micheau and M. Castaings, "Long Range Detection of Defects in Composite Plates Using Lamb Waves Generated and Detected by Ultrasonic Phased Array Probes," J. Nondestruct. Eval. **32**, 200-214 (2013).

[15] C. Potel, S. Baly, J.-F. de Belleval, M. Lowe and P. Gatignol, "Deviation of a monochromatic Lamb wave beam in anisotropic multilayered media: asymptotic analysis, numerical and experimental results," IEEE Trans. Ultrason. Ferroel. Freq. Contr. **52**, 987-1001 (2005).

[16] B.A. Auld, *Acoustic fields and waves in solids* (Wiley, New York, 1973), Vol. **1**, pp. 108-123.

[17] J.L. Rose, *Ultrasonic waves in solid media* (Cambridge University Press, Cambridge, 1999), pp. 33-37.

[18] K.Y. Kim, K.C. Bretz, A.G. Every, W. Sachse, "Ultrasonic imaging of the group velocity surface about the cubic axis in silicon," J. Appl. Phys. **79**, 1857-1863 (1996).

[19] B. Audoin, C. Bescond, M. Dechamps, "Measurement of stiffness coefficients of anisotropic materials from pointlike generation and detection of acoustic waves," J. Appl. Phys. **80**, 3760-3771 (1996).

[20] A.D. Degtyar, S.I. Rokhlin, “Comparison of elastic constant determination in anisotropic materials from ultrasonic group and phase velocity data,” J. Acoust. Soc. Am. **102**, 3458-3466 (1997).

[21] F. Reverdy, B. Audoin, “Elastic constants determination of anisotropic materials from phase velocities of acoustic waves generated and detected by lasers,” J. Acoust. Soc. Am. **109**, 1965-1972 (2001).

[22] J. Maris, “Enhancement of Heat Pulses in Crystals due to Elastic Anisotropy,” J. Acoust. Soc. Am. **50**, 812-818 (1971).

[23] M. Veidt, W. Sachse, “Ultrasonic point-source/point-receiver measurements in thin specimens,” J. Acoust. Soc. Am. **96**, 2318-2326 (1994).

[24] C. Prada, D. Clorennec, T.W. Murray, D. Royer, “Influence of the anisotropy on zero-group velocity Lamb modes,” J. Acoust. Soc. Am. **126**, 620-625 (2009).

[25] M. Youngjae, Y. Gyeongwon, K. Kyung-Min, R. Yuji, K. Young, “Comparison of slowness profiles of Lamb waves with elastic moduli and crystal structure in single crystalline silicon wafers,” J. Korean Soc. Nondestruct. Test. **36** (2016).

[26] M.A. Hopcroft, W.D. Nix and T.W. Kenny, “What is the Young’s Modulus of Silicon?,” J. Microelectromech. Syst. **19**, 229-238 (2010).

[27] B. Pavlakovic, M. Lowe, D. Alleyne, and P. Cawley, "DISPERSE: A general purpose program for creating dispersion curves," in *Review of Progress in Quantitative Nondestructive Evaluation*, edited by D.O. Thompson and D.E. Chimenti (Plenum, New York, 1997), Vol. **16**, pp. 185-192.

[28] M. Pizzolato, B. Masserey, J.-L. Robyr and P. Fromme, “High frequency guided wave propagation in monocrystalline silicon wafers,” in *Proceedings of SPIE*, edited by T. Kundu (SPIE, Washington, 2017), Vol. **10170**, 101702B.

[29] J. Virieux, “P-SV wave propagation in heterogeneous media: Velocity-stress finite-difference method,” Geophysics **51**, 889–901 (1986).